Dynamical and Structural Aspects of the Cold Crystallization of Poly(dimethylsiloxane) (PDMS)

Reidar Lund,*,† Angel Alegría,‡ Luis Goitandía,‡ Juan Colmenero,†,‡ Miguel A. González,§,|| and Peter Lindner§

Donostia International Physics Center, Paseo Manuel de Lardizabal 4, 20018 Donostia-San Sebastián, Spain, UPV/EHU, Departamento de Física de Materiales/Centro de Física de Materiales (Centro Mixto CSIC−UPV/EHU)), Paseo Manuel de Lardizabal, 3, 20018 Donostia, San Sebastián, Spain, Institut Laue-Langevin, 6, Rue Jules Horowitz, BP 156, F-38042 Grenoble Cedex 9, France, and Instituto de Ciencia de Materiales Aragón, CSIC−Universidad de Zaragoza, 50009 Zaragoza, Spain

Received September 12, 2007; Revised Manuscript Received November 20, 2007

ABSTRACT: A detailed study of the dynamical and structural aspects of the cold crystallization behavior of highly flexible poly(dimethylsiloxane)(PDMS) is presented. In order to understand the complete behavior, before, under and after crystallization, a wide range of experimental techniques have been employed. A particular emphasis is made on the interplay between dynamical and structural effects and how the properties of the amorphous phase evolve during the crystallization. This is highlighted by combining mobility sensitive techniques, involving broadband dielectric spectroscopy (BDS) and differential scanning calorimetry, with neutron scattering: wide and small-angle neutron scattering (WANS/SANS) which are sensitive to the relative ordering of the atoms. In this way, we are able to compare the structure associated with crystal formation with the evolution and modification of the amorphous phase. The kinetics deduced from WANS points toward a classical nucleation and growth behavior closely following a Avrami-like growth with an exponent of about $n = 3$ which is expected for athermal nucleation from fixed centers followed by three-dimensional crystal growth. Furthermore, the amorphous phase (deduced from BDS) decays in parallel with the emergence of the crystalline phase (from WANS/SANS) without any shift in the characteristic relaxation time. However a careful comparison of the crystallization at short times indicates that the amorphous phase seems to be affected before any measurable crystallization is detected by WANS. Although this might be compatible with the existence of mesomorphic phase, it may also be attributed to more simple precursors as initial crystalline "baby-like" nuclei. In this picture, these crystalline nuclei may be formed homogeneously in the system which in turn causes a constraint on the surrounding chains connected to these crystalline nuclei. This is manifested as a distinct relaxation contribution that is drastically slower and heterogeneous than the conventional amorphous α-relaxation of the melt. It would also explain a signal in SANS before any accompanying crystallization signal in WANS. Once the crystal starts developing, the fraction of the slower amorphous phase (constrained amorphous phase, CAP) grows and the conventional amorphous phase gradually disappears. At the very end the growing crystalline fronts start to overlap and some of the remaining CAP becomes even more constrained due to cross-link strongly manifested in both the dielectric response and the heat capacity.

1. Introduction

Despite being one of the most extensively studied branches of polymer physics, the complete physical picture of the crystallization process of polymers is far from complete.[1−3] This is mostly related to the fact that crystallization involves a subtle combination of equilibrium (thermodynamic) and nonequilibrium (kinetic) effects which are particular complex for polymers. Given the connectivity between segments, the dynamics of polymers is inherently slow which complicates and kinetically counteracts the crystal formation. This results in a rather complex hierarchically ordered structure which generally consists of a lamellar substructure having alternating amorphous and crystalline layers (interlayer distance of the order of nanometers) which then, on a larger scale, add up to form interpenetrated spherulites.[4] Recently, strong evidence has been provided suggesting that the lamellar structure display a granular substructure mediated by more constrained amorphous like interfacial regions.[2,5]

A very important issue associated with the polymer crystallization is the dynamical and structural properties of the amorphous phase and how it is modified by the crystallization. Concerning dynamics, this question is of strong general interest in itself as the lamellar structures act as confining templates of the polymer chains in the nanometer range. From a more practical point of view, the amorphous phase is essential for the stability as well as for the structural and mechanical properties of the final semicrystalline material. This is because the mediating amorphous chains would act as cross-links through tethering, lamellar spanning, and entanglements. Concerning kinetics of crystallization, mesomorphic structures may be an important intermediate pre-ordering step having a much smaller activation energy which according to Ostwald step rule will eventually transform into the stable crystal.[2,3,6] Some approaches favor the initial formation of bundle-like entities[3] display some degree of ordering but have a much higher entropy than the final crystals, while other approaches considers a sort of thermodynamical spinodal-like liquid−liquid decomposition prior to crystallization.[7−9] Such features would imply a more complex mechanism than the classical nucleation and growth

* E-mail: reidar_lund@ehu.es.
† Donostia International Physics Center.
‡ UPV/EHU: Departamento de Física de Materiales/Centro de Física de Materiales (Centro Mixto CSIC−UPV/EHU)).
§ Institut Laue-Langevin.
|| Instituto de Ciencia de Materiales Aragón, CSIC−Universidad de Zaragoza.

10.1021/ma702055b CCC: $40.75 © 2008 American Chemical Society
Published on Web 01/26/2008

picture where the crystals initially grow from a critical nucleus ignoring any restructuring processes or intermediate steps. Mesomorphic structures have indeed been directly observed experimentally in certain systems[2,3] such as in poly(ethylene) (PE) where a thermotropic hexagonal phase is observed prior to the formation of the most stable ortorhombic crystalline phase. Using wide-angle X-ray scattering (WAXS) and careful data modeling, it has also been demonstrated directly that the amorphous phase of PE undergoes strong modifications under crystallization which cannot properly be described unless a third intermediate phase is introduced.[10] On the other hand, a combined study[11] of simultaneous small and wide-angle X-ray scattering (SWAXS) of isotactic poly(propylene) has favored the classical nucleation and growth picture, at least for this polymer. The same more classical view has also been favored from computer simulations.[12,13]

Apart from structural techniques as X-ray/neutron scattering, a very powerful way to study crystallization and the associated modification of the amorphous phase is via techniques sensitive to the local mobility such as broadband dielectric spectroscopy (BDS),[14,15] which provides a better sensitivity to the amorphous phase. A recent BDS study has shown that by investigating both the segmental α and the local β process simultaneously, conclusion can be drawn indicating a sort of modified amorphous phase acting as precursor state before polymer crystals are formed.[15] Combining BDS and SAXS simultaneously, a recent study on the warm crystallization of poly(caprolactone)[16] has indeed shown that the amorphous phase is modified before any associated change in the SAXS curves can be detected. This has been interpreted as a signature of a pre-ordering process preluding the crystal formation. Other studies on another polymer system, poly(ethylene terephthalate)(PET), employing both BDS and SWAXS simultaneously[17,18] have shown that the mobility of the amorphous phase is not significantly affected during primary crystallization but the strongest effect appears after the onset of the secondary crystallization. It is interesting to note that, in BDS, a continuous broadening and shifting of the relaxation loss peak toward lower frequencies are usually observed.[19−22] However in some cases the position and shape of the α-relaxation peak remains constant and just decays in intensity while it is gradually replaced by a second slower peak at lower frequencies. It has been suggested[20] that such behavior is associated with polymers with high intrinsic chain flexibility such as poly(L-lactic acid) (PLLA),[19] poly(3-hydroxybutysrate)-(PHB),[20] etc.

In this study we present a detailed study of the cold crystallization process of one of the most flexible polymers known: poly(dimethylsiloxane) (PDMS). Because of the molecular symmetry and small side groups PDMS crystallizes easily, but owing to the high flexibility, this occurs only at low temperatures below the melting region (below 220−250 K). As a consequence there have only been few studies on the crystallization behavior of this polymer. Previous studies have mainly been focused on the structural properties[24−26] of PDMS while only some few studies have been devoted to the kinetical properties under crystallization from solution[27] and in bulk.[28,29] Concerning dynamics, it is well established[30−32] that crystallization of PDMS leads to a modified amorphous phase that due to its slower dynamics, can be designated as "rigid amorphous phase" (RAP) or more precisely "constrained amorphous phase" (CAP). However the evolution of the behavior and its role during crystallization have not been investigated so far. Recently a study of pure PDMS and nanosegregated poly(styrene)-PDMS (PS−PDMS) diblock copolymers have revealed that the confinement of PDMS into lamellar phases has qualitatively the same effect as crystallization[23] leading to an extra well-separated CAP related relaxation at low frequencies which we may call the α_c-process. This was attributed to a tethering/anchoring effect rather than a geometrical finite size and confinement effect.

The rather clear separation in time scale of the dielectric contributions from the conventional AP and CAP provides a convenient way to investigate in detail the evolution of the dynamics of both disordered amorphous parts during crystallization. Thus, we here combine various experimental techniques to simultaneously look on the dynamical and structural features of PDMS undergoing crystallization. The aim is twofold: first, further elucidate the effect of confinement and restriction of the amorphous phase, and second, understand the role of the constrained amorphous phase (CAP) during crystallization with particular reference to potential mesomorphic/precursor phases. The structural properties have been investigated using small and wide angle neutron scattering (SANS/WANS) allowing a direct determination of the crystallinity and details about molecular and mesoscopic crystal parameters (lattice and lamellar parameters). In turn these results are combined with independent results of the dynamics obtained from broadband dielectric spectroscopy and differential scanning calorimetry (DSC). BDS is particular useful for PDMS as the large dipole moment of the monomer units provides a strong dielectric signal. As this technique provides detailed information about segmental mobility, DSC provides insight into the overall degree of freedom of the chains as well of the general thermodynamical behavior. Special emphasis has been made to the isothermal crystallization kinetics, which has been determined in situ using all the above-mentioned techniques.

2. Experimental Section

In this section, we present the essential experimental details concerning the material and the techniques employed in this study.

2.1. Materials. The deuterated PDMS sample (d-PDMS) sample employed in this work was purchased from Polymer Source Inc. (Product ID: P3413-dDMS) and used as received without any further treatments. The sample was characterized by gel permeation chromatography (GPC) using 4 columns of the type PLgel (5 μm Mixed D) from Polymer Laboratories (now Varian), toluene as solvent and a flow rate of 1 mL/min. The results demonstrate a number-average molecular weight M_n of 74 000 g/mol and a polydispersity $M_w/M_n = 1.76$ (M_w denotes the weight-average molecular weight).

2.2. Differential Scanning Calorimetry. The calorimetric measurements were carried out using a Q1000 TMDSC from TA Instruments. The sample mass for these measurements was about 8−10 mg. Samples were encapsulated in standard hermetic aluminum pans and a gas flow (He) was used for thermalization. Correction of asymmetry relative to reference pan, difference in aluminum pan weight, etc. was performed using the standard procedure of online correction for the DSC Q1000 ("TzeroTM method"). For the temperature modulated DSC measurements, used for the investigation of the kinetics of crystallization, the sample capsule was quenched in liquid nitrogen outside the instrument and rapidly inserted into the sample holder of the instrument once the temperature had stabilized at 123 K.

2.3. Wide Angle Neutron Scattering (WANS). The wide angle neutron scattering experiments were performed using the D1B two-axis powder diffractometer at Institute Laue Langevin (ILL), Grenoble, France. D1B is equipped with a position sensitive detector consisting of 400 detector element units located 0.2 °C apart along the θ scattering angle. The instrument is operated in a high flux mode with medium resolution allowing a simultaneous recording of the diffraction spectra over a wide interval of θ range of $10 \leq$

$\theta \leq 90°$. The optimal flux was achieved using an incoming neutron beam with wave length of $\lambda = 2.522$ Å monochromated using a pyrolytic graphite single crystal. This setup allowed a rather broad Q range of $0.26 \leq Q \leq 3.39$ Å^{-1} ($Q = 4\pi \sin(\theta/2)/\lambda$) where θ is the scattering angle.

The sample was prequenched in liquid nitrogen before loaded cold into the cryostat that allowed a temperature regulation better than ±0.2 K. In order to achieve a good comparison with the other experiments, the temperature was calibrated with carbon disulfide, CS_2, which shows a sharp melting temperature at 161.6 K. The results show that for the current cylindrical vanadium sample holder, the temperature off-set was $\Delta T \approx 1$ K relative to the nominal sample temperature read-off.

2.4. Small-Angle Neutron Scattering (SANS). The SANS-measurements were carried out at the D-11 instrument at ILL in Grenoble, France. The measurements were performed at several detector-to-sample distances and collimation lengths covering an extended Q range. As the investigated samples are relatively weak scatterers and the primarily focus of this work concerns kinetics, the resolution conditions were relaxed in order to gain in flux. This was achieved by choosing a rather large circular beam with a diameter of 13 mm and collimation distance of 10.5 m ($L = 10$ m detector distance), 5.5 m ($L = 5$ m), 2.5 m ($L = 2.5$, and $L = 1.1$ m). The wave length was chosen to be $\lambda = 5$ Å ($\Delta\lambda/\lambda \approx 0.09$). The modulus of the wave-vector, Q thereby takes values in the range of approximately: 8.3×10^{-3} Å$^{-1} \leq Q \leq 0.4$ Å^{-1}. detector sensitivity corrections were made using water. Water was also used as secondary standard after being precalibrated with vanadium. Background noise on the detector was measured using a piece of solid cadmium (Cd) to block the primary beam. All background substraction was done directly pixel by pixel on the two- dimensional detector intensity image. After radial averaging the intensities were treated for dead time effects using standard approaches in order to yield the absolute normalized macroscopic differential scattering cross sections $d\Sigma/d\Omega(Q)$. For more detailed description see for example Chapter 2 of ref 34.

In order to calibrate the temperature, the scattered intensity of the sample itself or, more precisely, the count rate of the detector monitor was observed over all the temperature range. The temperature where most of the small angle scattering vanishes, was taken as the melting temperature. Comparison of the value from DSC revealed an apparent offset of approximately $\Delta T \approx 2$ K.

2.5. Broad Band Dielectric Spectroscopy (BDS). The complex dielectric permittivity $\epsilon^* = \epsilon' - i\epsilon''$ vs frequency was measured in a frequency range between 10^{-2} and 10^7 Hz using a Novocontrol high-resolution dielectric analyzer (Alpha-S analyzer). The PDMS sample has a low viscosity at room temperature and can be prepared directly between two gold-plated electrodes of diameter: 20 and 30 mm, respectively. Subsequently the samples were degassed and dried by placing them in a vacuum oven and then squeezed between the plates using a finely cut 0.1 mm star-formed Teflon piece as spacer. Finally before being inserted into the instrument, the samples were briefly placed under vacuum for some minutes to avoid any trapped air bubbles.

The data were measured in a temperature range between 140 and 240 K and the temperature was controlled within $\Delta T = \pm 0.1$ K using a Novocontrol Quatro cryostat. In order to avoid crystallization upon cooling, the samples were quenched in liquid nitrogen before placed in the cryostat prethermostated at 140 K. Subsequently, for the kinetic measurements, the temperature was raised slowly avoiding any overshoot until reaching the crystallization temperature.

3. Results

3.1. Differential Scanning Calorimetry (DSC). In order to characterize the thermal properties of the system, standard differential scanning calorimetry (DSC) was first used. Figure 1 shows a typical scan of the heat flow as a function of temperature upon heating with a rate of 2 K/min. As seen the data demonstrate a clear glass transition temperature at $T_g \approx$ 146.5 K. Further increasing the temperatures we observe a crystallization peak at about 181 K before a rather broad melting transition with multiple peaks which is observed in the temperature range between 218 and 238 K. In the following we will focus on the temperature range between the glass transition and the cold crystallization temperature. Here the crystallization of the supercooled amorphous liquid is thermodynamically strongly favored but kinetically inhibited (cold crystallization range).

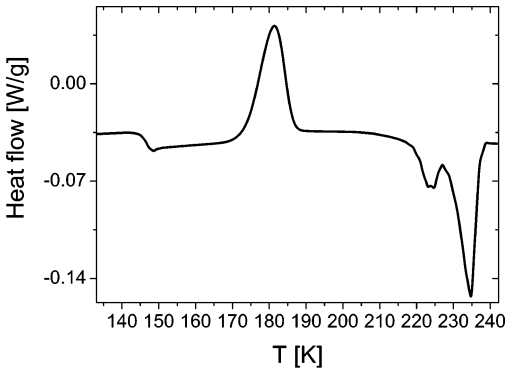

Figure 1. Differential scanning calorimetry (DSC) trace of d-PDMS showing the specific heat flow as a function of temperature. The heating curve shows a clear glass transition temperature at around 146.5 K, a cold crystallization temperature, T_{cc}, at around 181 K, and finally a rather broad melting region in between 218 and 238 K.

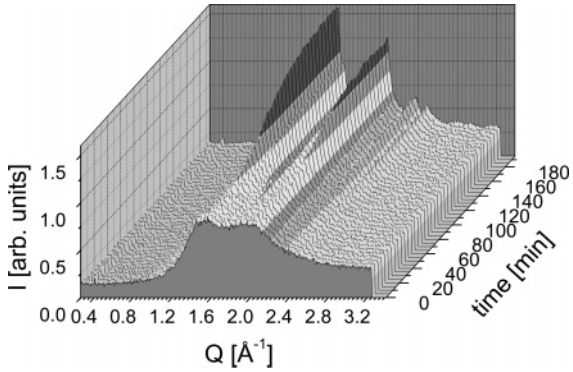

Figure 2. Time evolution of wide angle neutron scattering patterns of d-PDMS undergoing crystallization at 163.4 K.

3.2. Wide Angle Neutron Scattering (WANS). The evolution of crystals from a fully amorphous state can be directly seen by time-resolved WANS under isothermal conditions sufficiently above T_g. This is demonstrated in Figure 2 which displays the time evolution of the WANS pattern as a function of time obtained at 163.4 K after heating from an initial glassy amorphous state. As seen the scattering evolves from a rather diffuse, broad scattering pattern at short times to well-defined Bragg peaks visible above the amorphous scattering at longer times.

The scattering of the amorphous and crystalline part is presented in more detail in Figure 3. Comparing the data of the semicrystalline state shown in Figure 3b, with the results of Albouy,[25] we see a very good coincidence of all peak positions except the first reflection (0.1.1) at approximately $Q \approx 0.91$ Å^{-1} which is not present in our data. This may simply come from the fact that in the former study the sample has been stretched and partially aligned using silica fillers whereas the current sample is quenched into disorder and let crystallized from cold temperatures. Accordingly we may assign the crystalline structure of PDMS to be a fourfold helical configuration ordered in a tetragonal lattice which was recently

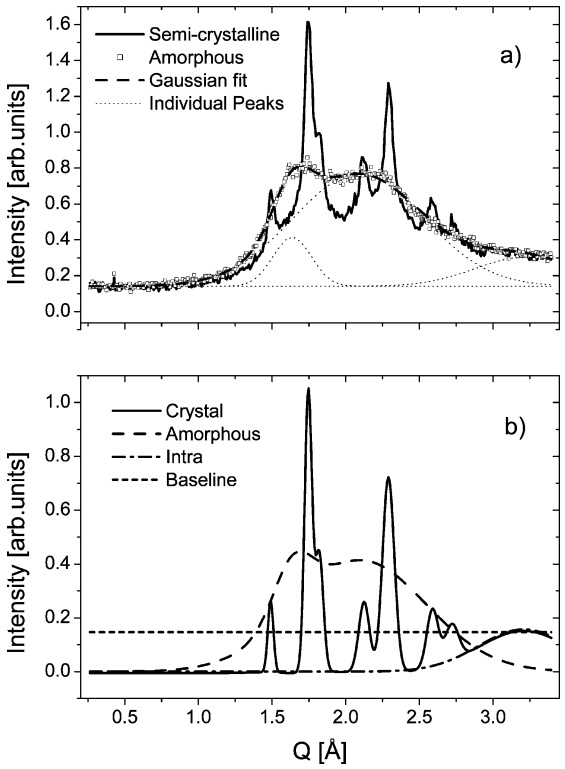

Figure 3. Scattering of the amorphous and semicrystalline state at 162.4 K: (a) scattering of the initial fully amorphous state (symbols) and the fuly semicrystalline state (full lines). Dotted lines correspond to the individual Gaussian peaks used to describe the amorphous phase. The broad peak at highest Q was designated the intramolecular contribution. Broken line displays the fit to the sum of all three peaks. (b) Components of the scattering of the semicrystalline structure at the final stage. Total crystal contribution (solid line) together with the individual contributions of the amorphous fraction (dashed line) and the intramolecular part (dash-dotted line). Baseline is represented by the short dashed lines.

proposed[25] to replace the originally accepted monoclinic structure.[24] As a first step to analyze the kinetics of crystallization, the relative degree of crystallinity was estimated evaluating the area under the second and third peaks ((1.2.1) and (0.1.3) reflections respectively following ref 25). This was done by directly calculating the area in the range $Q = 1.6008-1.9344$ Å^{-1} for all times. The results of the analysis are given in Figure 4.

In order to estimate the absolute degree of crystallization and provide more accurate data, the amorphous and crystalline scattering have to be deconvoluted and fitted over a larger Q range. As the peaks of the amorphous and the crystalline part greatly overlap, the data were fitted to the simplest possible two phase model. A simple but robust way to do this is to describe the scattering of each part as a sum of standard Gaussian functions:

$$I(Q) = \sum_i \frac{a_i}{w_i\sqrt{2\pi}} \exp(-(Q_i - Q)^2/2w_i^2) \qquad (1)$$

where a_i is the relative amplitude and w_i is the width and Q_i is the center of the individual Gaussian peaks. First, the scattering of the fully amorphous phase ($I_{am}(Q)$) was parametrized using a sum of three Gaussian functions as depicted in Figure 3a). Note that both the amorphous and semicrystalline sample coincide at large Q which must be related to a scattering term originating from intramolecular correlations that do not seem

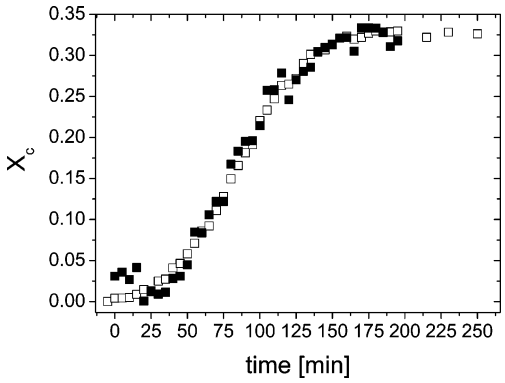

Figure 4. Time dependence of the crystallinity using the area and deconvolution methods. The first "area method" (filled squares) display the results using only the integrated intensity under the second and third peaks ((1.2.1) and (0.1.3) reflections respectively following ref 25) The open squares represent the results from the analysis using a deconvolution of the total scattering signal into an amorphous and a crystalline part (see eqs 1 and 2). The former data from the area analysis method, which gives only the relative crystallinity, have been scaled to the absolute crystallinity determined from the deconvolution method to facilitate a comparison.

to change from the crystal to the amorphous state. It is therefore reasonable to fix the third peak function ($I_{intra}(Q)$) as common in both the amorphous and semicrystal phase. In addition the background scattering (I_{BG}) originating from parasitic scattering, gamma particles/unmoderated fast neutron, electronic noise etc. has to be added. As a second step, the crystal scattering ($I_c(Q)$) was described by adding seven additional Gaussian peak functions describing the Bragg reflections of the crystal and fitted to the final state by a simple superposition with the amorphous part. Thus, in the following way we can describe the scattering of the semicrystalline state in terms of the crystallinity fraction X_c and write the total scattering as

$$I(Q) = (1 - X_c(t))I_{am}(Q) + X_c(t)I_c(Q) + I_{intra}(Q) + I_{BG} \qquad (2)$$

The resulting fit together with the individual contributions of the amorphous and crystalline phase are depicted in Figure 3. In the analysis of the kinetics of crystallization, the only parameter allowed to vary was $X_c(t)$. The parameters of the amorphous and crystal scattering were fitted using the initial and final state respectively, and at all intermediate times the widths, relative amplitudes and peak positions were held fixed. The excellent quality of the fits implies that neither the individual amorphous nor the crystalline structure seem to change significantly with time or temperature. The time evaluation of the crystallinity fraction, $X_c(t)$ is compared with the "area-method" in Figure 4. As seen both methods show the same functional behavior, but the deconvolution method yields data with better precision, and, very importantly, in terms of absolute values. Subsequently, the second, latter method was used at all other temperatures and the results are displayed in Figure 5a . It should be noted that the description of the scattering of the amorphous phase is a qualitative one and not an accurate physical description. Concerning the description of the crystalline fraction, the intramolecular component is not well-defined, and care must be taken in order to not introduce systematic errors in the absolute crystallinity. In order to avoid any ambiguity, the intensity curves were evaluated by fitting the first 200 points in the reduced Q range of 0.26−1.96 Å^{-1}. However, as exemplified for $T = 158.4$ K in Figure 5a, this has only a minor impact on the data. Furthermore, we also here assume that the amorphous local conformation is unaffected by the crystallization and can be described by the constant set of

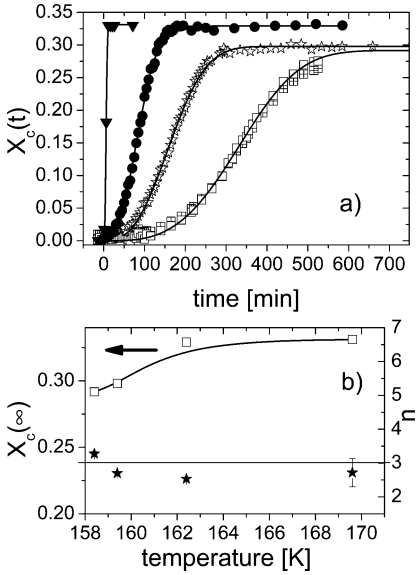

Figure 5. (a) Time evolution of the crystallinity fraction, $X^{WANS}(t)$, for different temperatures as determined by WANS. From left to right: 169.4 K (triangles), 162.4 K (filled circles), 159.4 K (stars), and 158.4 K (squares). For the latter temperature, the results from fitting the complete Q range and the first 200 points have been included as crossed and open squares respectively (see text for details). The solid lines display fits to the Avrami equation. (b) Temperature dependence of the power exponent, n (right), and the final crystalline fraction $X^{WANS}(\infty)$ (left) deduced by the fitting the Avrami equation (eq 3) to the experimental data. The lines only serve as a guide for the eye.

three Gaussian functions. However given the limited resolution of this experiment and the excellent description of data, shown in Figure 3, the data analysis can be safely regarded as very satisfactorily. Hence a three phase model which has been used in the case of PE,[10] where the amorphous and crystalline peaks are more well-separated, is not justified in this case.

In order to quantify the kinetics the classical Avrami equation was fitted to the experimental data:

$$X_c(t) = X_c(\infty)(1 - \exp(-(kt)^n)) \quad (3)$$

The results of the fits are given in Figure 5a and the corresponding fit parameters: $X_c(\infty)$ and n are given in Figure 5b. As seen, the Avrami exponent, n, takes values of about 3, in the range of 2.7−3.2 which is compatible with values reported for PDMS in crystallization from solution and bulk ($n \approx 1.7-3.1$).[33]

3.3. Small-Angle Neutron Scattering (SANS). The small angle scattering curves of d-PDMS obtained at different temperatures after quenching the sample in liquid nitrogen are depicted in Figure 6.

As seen all curves, including the data at 248 K, which is above the melting point, display a strong low Q scattering that approximately follows a power-law like Q^{-x} dispersion with exponent, x of about 2.8. This probably results from large scale heterogeneities that can be related to impurities, air bubbles, aggregates, microvoids etc. More importantly, as seen in the intermediate Q range, a correlation peak develops in the spectra above 160 K. This is a typical signature of periodic lamellar structures where the mean lamellar spacing is given by $d_{lam} = 2\pi/Q_{peak}$ where Q_{peak} is the position of the peak maximum. In order to describe the data over the whole Q range we fitted the data to a similar phenomenological function as by Wang et al.[11] Here we consider three terms: a constant background, I_{BG}, the contribution from the large scale impurities $I_D(Q)$ and the scattering from the assembly of alternating lamellar structures.

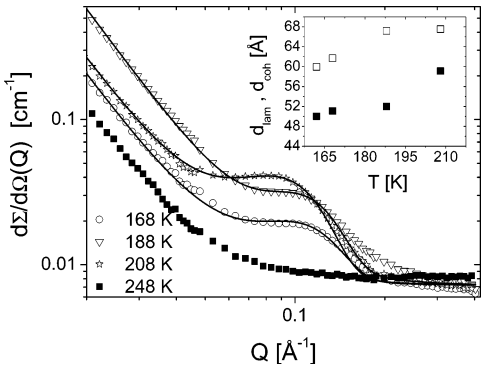

Figure 6. Small angle scattering curves of d-PDMS at different temperatures. The data has been obtained after first quenching the sample in liquid N_2 and subsequently gradually heated to the indicated temperatures. The inset plot display the inter lamellar spacing distance, d_{lam}, (filled squares), and the coherence length of the lamellar structure, d_{coh} (open squares), as a function of temperature (see text for details).

The latter is approximately given by the product of the individual lamellar form factor and the lattice structure factor divided by the factor Q^2 taking into account the random orientation of the crystallites. By considering a simple power law for the low Q scattering, we end up with the following expression:[11]

$$d\Sigma/d\Omega(Q) = AQ^{-x} + BP_{lam}(Q)S_{lam}(Q)/Q^2 + I_{BG} \quad (4)$$

where A and B are numerical prefactors and $P_{lam}(Q)$ is the form factor for a one-dimensional lamella with width w given by $P_{lam}(Q) = |\sin(wQ/2)/(wQ/2)|^2$. For sake of simplicity we approximate the structure factor of the periodic lamellar structure by a Gaussian function with a width, σ_{lam}: $S_{lam}(Q) = \exp(-(Q - Q_{peak})^2/2\sigma_{lam}^2)$.

In order to minimize the amount of variables, x were first fitted and kept constant to $x = 2.8$, which corresponds to a typical near three-dimensional mass-fractal that could be particles arising from impurities etc. Because of the limited resolution of the experiment, finer structural features such as the lamellar thickness cannot be determined with accuracy. However values were found in the region of $w \approx 10-25$ Å, and display some indication to increase with temperature. From the width of the Gaussian structure factor peak we find a value of about $\sigma_{lam} \approx 0.05-0.03$ Å^{-1} which is significantly larger than the width corresponding to the experimental resolution: $\sigma_Q \approx 6 \times 10^{-3}$ Å^{-1}.[35,36] However, since the resolution function essentially is a Gaussian, the corrected width can be calculated as: $\sigma'_{lam}{}^2 = \sigma_{lam}{}^2 - \sigma_Q{}^2$. Using these values we can can calculate the coherence length of the crystal, $d_{coh} = 2\pi/\Delta Q$ where ΔQ is the total width of the peak (fwhm (full width at half-maximum) value). For a Gaussian peak function we thus obtain d_{coh} according to

$$d_{coh} = \frac{2\pi}{\sigma'_{lam}\sqrt{8 \ln 2}} \quad (5)$$

Inserting the values obtained, we calculate $d_{coh} \approx 59-67$ Å-values which are comparable to the typical inter lamellar periodic distances, as shown in the inset plot in Figure 6.

In analogy with WANS, the crystallization kinetics was also monitored using SANS. However, at 160 K and below, the kinetics was unpractically slow and significant structural changes could only be followed at 162 K. The results are shown below in Figure 7 for selected times.

It is interesting to note that the correlation peak between the lamellar regions (at about 0.1 Å^{-1}) seems to grow uniformly in

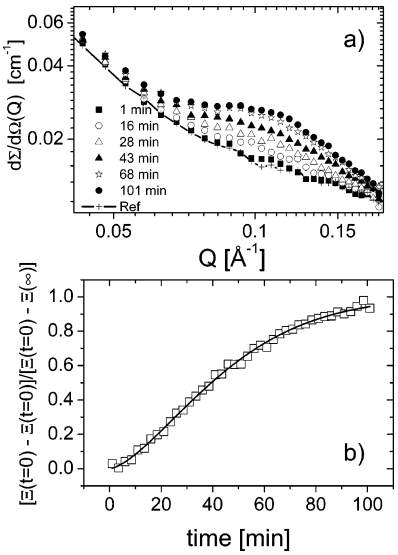

Figure 7. (a) Evolution of the small angle scattering curves of d-PDMS at 162 ± 1 K. The reference curve displays the scattering before any significant crystallization has taken place. (b) Normalized invariant as a function of time. The line represents a fit to an Avrami-like growth law (see text for details.)

intensity with time without any significant shift in Q. In order to obtain a more quantitative description, the time evolution of the "invariant", Ξ was calculated over the experimental Q range at this detector setting: $Q_{min} = 0.028 \leq Q \leq Q_{max} = 0.183$ Å^{-1}.

$$\Xi = \int_{Q_{min}}^{Q_{max}} Q^2 I(Q)\, dQ \tag{6}$$

The time evolution of the normalized invariant $((\Xi(t) - \Xi(\infty))/(\Xi(t=0) - \Xi(\infty)))$ is displayed in Figure 7b. For a two-phase system the invariant should ideally scale like:[34] where $\Xi \sim (1 - X_c(t))X_c(t)$ when we assume that the difference of the scattering length density (or equivalently the density) between the crystal and amorphous phase is constant during the crystallization which indeed is supported by the WANS result. We can thus using eq 3 fit the data on the form: $(\Xi(t=0) - \Xi(t))/(\Xi(t=0) - \Xi(\infty)) = a(1 - \exp(-(kt)^n))(1 - (1 - \exp(-(kt)^n)))$, where a is a numerical constant close to 1. After fixing this latter value to 1, we obtain $n \approx 1.5$ and a rate constant of $k \approx 0.012$ min^{-1}. Using a plain Avrami function, we obtain similar n. In any case we see values of n that are much lower than that was found from WANS which may indicate that the implicitly assumed two-phase model is not valid.

3.4. Broad Band Dielectric Spectroscopy (BDS). The frequency dependency of the dielectric loss permittivity, ϵ'' is depicted in Figure 8 at different temperatures for two different thermal histories. Focusing on Figure 8a, which shows the behavior upon heating starting from fully amorphous glass, we observe a well-defined loss peak associated with the structural alpha relaxation time strongly moving toward higher frequencies with the temperature. At temperatures above about 158 K, we observe a low-frequency tail that gradually gets more pronounced and finally at 164 K develops into a broad peak coexisting with the conventional α-relaxation peak. At the same time, the conventional α-relaxation decreases in intensity. At 166 K the conventional α-relaxation vanishes and only this slower and very broad process, which we may call α_c, remains. The emergence of this process is clearly associated with the crystallization and can bee seen more clearly in Figure 8b. This shows the temperature evolution of the α_c-process between 156 and 180 K obtained upon gradual cooling from 180 K where the cold crystallization process is complete. As seen, the α_c-process is here very broad and much slower than the conventional α-relaxation. Following earlier experimental work we may associate this relaxation with a "constrained amorphous phase" (CAP) which is related to more restricted amorphous chains confined and connected between polymer crystallites.[23,30−32]

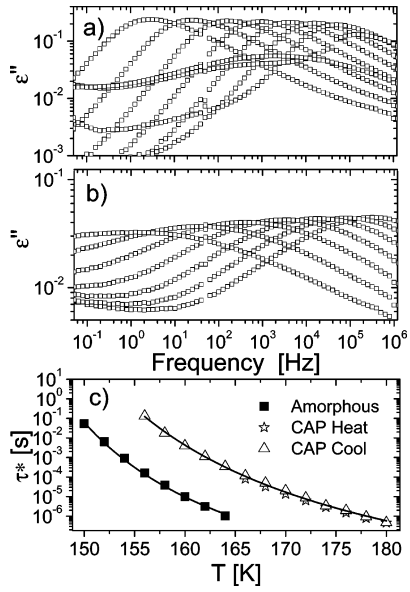

Figure 8. Dielectric loss permittivity, ϵ'' of d-PDMS as a function of frequency after: (a) quenching the sample to liquid N_2 temperature and progressive heating in the range of 150−166 K with a 2 K increment-(from left to right) and (b) temperature range between 156 and 180 K with 4 K increments (from left to right) obtained upon gradually cooling the sample down from 180 K. Part c displays the temperature dependence of the characteristic time, τ^* for the amorphous phase prior to crystallization (solid squares), and the "CAP" phase upon progressive heating (open stars) as well as the "CAP" after completed crystallization at 180 K and subsequent cooling (open triangles). The solid lines display fits to the Vogel−Fulcher−Tamman (VFT) equation (eq 7).

Table 1. Characteristic Parameters of the α-Relaxation of the Conventional and Restricted Amorphous Phase (AP/CAP) of PDMS[a]

phase	B	T_0/K	T_g ($\tau = 100$ s)/K	m
AP	482 ± 43	131 ± 2	145 ± 1	154
CAP	707 ± 51	128 ± 2	150 ± 1	95

[a] The glass transition temperature, T_g, is estimated based on the condition $\tau^* \equiv 100$ s. The fragility index, m is calculated based on eq 8 (see text for details). The value for τ_0 was fixed to $\tau_0 = 5.5 \cdot 10^{-13}$ s according to Ref[23]

The temperature dependence of the most probable time (corresponding to the maximum of the distribution function), $\tau^* = 1/(2\pi f^*)$, is determined from the position of the maxima (f^*) of the dielectric loss permittivity and is given for the two processes in Figure 8c.

The temperature dependence can in both cases be described by a typical Vogel−Fulcher−Tamman (VFT) law:

$$\tau^* = \tau_0 \exp(B/(T - T_0)) \tag{7}$$

where T_0 is the characteristic temperature, where τ^* values tend to diverge, τ_0 is the characteristic shortest time in the system, and B is a parameter describing the temperature dependence. The obtained values are listed in Table 1.

As seen in Figure 8c, τ^* can be excellently described with the VFT equation for both the relaxation in the conventional amorphous phase as well as the "constrained amorphous phase". As is customary in the general concept of glass forming liquids,

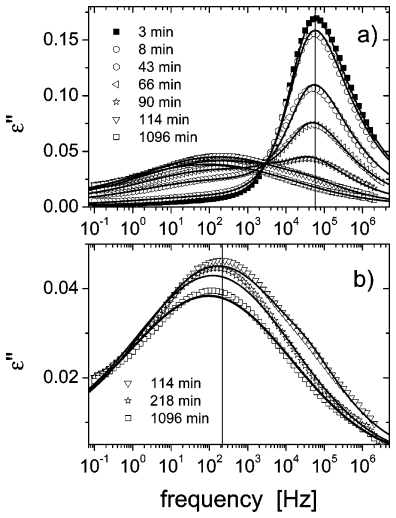

Figure 9. (a) Time evolution of the dielectric loss permittivity, ϵ'', as a function of frequency at 162 K. The solid lines corresponds to the fit using a linear superposition of the response of the amorphous phase and the CAP (for details, see text). (b) Same data corresponding to the large times as in part a, where the most of the relaxation stems from the CAP. Vertical lines are meant as guides for the eye only.

we can also calculate the fragility index, *m*, defined by Angell.[38] Assuming the validity of the VFT law, this value is given by

$$m = \frac{B}{T_g \ln(10)(1 - T_0/T_g)^2} \quad (8)$$

Inserting the values from the VFT fits and defining T_g as the temperature of which $\tau(T_g) = 100$ s, we see that the index of the amorphous PDMS ($m \approx 154$) is considerably larger than that for the CAP phase ($m \approx 95$). This demonstrates a "stronger" character of the latter CAP phase suggesting a more constrained local environment.

The effect of crystallization on the dielectric response is also evident in a real time experiment under isothermal conditions. The result of such an experiment at 162 K, where the crystallization process proceeds relatively fast, is given in Figure 9.

As seen, the spectra consist of practically one peak at short times and as the time evolves, a second much broader peak at lower frequency develops. Finally, the high frequency amorphous peak completely disappears, and only the broad relaxation peak characterizing the CAP is visible. Surprisingly, during crystallization, it seems that both peaks approximately keep their shape as well as peak position—only their respective amplitudes seem to vary. Consequently, at all times during crystallization, the $\epsilon''(\omega, t)$ can be described by a sum of two contributions, one for the ordinary α-relaxation of the conventional amorphous phase and one for the α_c-relaxation of CAP.

In order to parametrize the data, we chose to describe the "CAP" response, after complete disappearance of the conventional α-relaxation, using a sum of a general lognormal function, as this contribution is broad and symmetric. In addition we added a power law describing a small contribution that only occurs at very low frequencies and that cannot be resolved properly even at higher *T*. The α-relaxation before any signature of crystallization was described by a Havriliak−Negami (H−N) function. At all intermediate times, we describe the total dielectric loss signal as a linear superposition of the contributions of these two phases and the power-law term:

$$\epsilon(\omega, t)'' = a_{CAP}(t)(A\omega^{-x} + \epsilon''_{CAP}(\omega)) + a_{AP}(t)\epsilon''_{AP}(\omega) \quad (9)$$

Table 2. Parameters from the Fitting Procedure of the Data from Dielectric Spectroscopy[a]

T/K	$\Delta\epsilon_{AP}$	α	γ	$\tau_{AP}/10^{-6}$ s	$\Delta\epsilon_{CAP}$	σ_{AP}	$\tau_{CAP}/10^{-6}$ s
162	0.60	0.89	0.44	6	0.31	2.0	800
160	0.66	0.94	0.42	21	0.31	2.1	4400
158	0.70	0.98	0.41	79	0.35	2.2	25 300

[a] The parameters from the α-relaxation from the amorphous phase and the ones obtained from fitting the modified CAP α_c-relaxation in the semicrystalline phase have been fitted separately. The exponent *x* and the amplitude of the power law have been determined to be $x = 0.06$ and $A = 6.86 \times 10^{-3}$ respectively and were fixed to these values for the three temperatures.

Here *A* is an amplitude, *x* is a power exponent and a_i is the relative contribution (amplitude) of each dynamic phase. The CAP contribution is written as

$$\epsilon(\omega)''_{CAP} = \sqrt{\frac{8}{\pi}} \frac{\Delta\epsilon_{CAP}}{\sigma_{CAP} \ln 10} \exp(-\log(\omega\tau_{CAP})^2/2\sigma_{CAP}^2) \quad (10)$$

where τ_{CAP} and σ_{CAP} is the mean time and the width of the lognormal function respectively. The amorphous part is described by the following H−N equation:

$$\epsilon(\omega)''_{AP} = \mathrm{Im}\left[\frac{-\Delta\epsilon_{AP}}{(1 + (i\omega\tau_{AP})^{\alpha})^{\gamma}}\right] \quad (11)$$

where α and γ are the parameters describing the symmetric and asymmetric broadening respectively and τ_{AP} is the characteristic time.

As already mentioned above, each term was separately fitted to the experimental data corresponding to initial amorphous state and the semicrystalline state of which the conventional amorphous response completely vanishes ($a_{CAP} = 0$ and $a_{AP} = 0$ respectively). Thus, in eqs 10 and 11, $\Delta\epsilon_{AP}$ and $\Delta\epsilon_{CAP}$ are the dielectric strength obtained of the initial fully amorphous phase and that obtained after completed crystallization, respectively. The relevant data parameters are listed in Table 2.

Second, the superposition in eq 9 was used to fit data at all intermediate times by letting only $a_{AP}(t)$ and $a_{CAP}(t)$ vary. This worked well under the crystallization process until the conventional amorphous part completely vanishes $a_{AP} = 0$, after that we observe a slow evolution of the CAP contribution where the peak slightly moves toward slower frequencies (see Figure 9b). Consequently, at longer times, τ_{CAP} and σ_{CAP} were also allowed to vary.

The normalized total dielectric strength as a function of time is plotted in Figure 10a . The data was normalized by ϵ_∞ in order to cancel small differences in the sample geometry (thickness, etc.) and thereby facilitating a quantitative comparison of the different temperatures. The extracted amplitudes, a_{AP} and a_{CAP}, are depicted in Figure 10b.

In order to extract information about the kinetics, the decay of the conventional amorphous phase, represented by a_{AP}, was fitted using a general Avrami equation $a_{AP} = a \exp(-(kt)^n)$. As seen in Figure 10b, the data could not be described completely satisfactorily by this equation, especially at short times.

The above data demonstrate, as expected, a strong anti correlation between the disappearance of the conventional amorphous phase and the emergence of the CAP part. This indicates that the CAP is associated with the tethering of chains to the crystal fronts and/or the restrictions imposed by the crystal lamellas. This correlation becomes evident when observing that the sum $a_{CAP} + a_{AP}$ indeed remains essentially constant in time

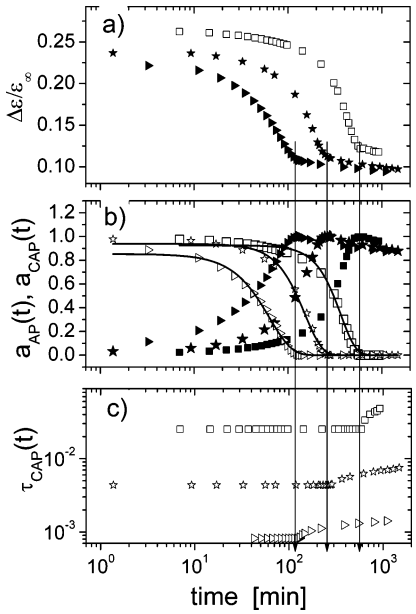

Figure 10. (a) Total normalized dielectric strength of d-PDMS as a function of time. $\Delta\epsilon = a_{AP}\Delta\epsilon_{AP} + a_{CAP}\Delta\epsilon_{CAP}$. The data have been normalized to the completely unrelaxed dielectric permittivity, $\epsilon(\infty)$ in order to correct for minor geometrical effects. (b) Amplitudes corresponding to the individual contributions to the dielectric strength of the amorphous phase (a_{AP}) (open symbols) and the "constrained amorphous phase" a_{CAP} (closed symbols). The solid lines represent fits of a general Avrami equation (see text for details). (c) Evolution of the characteristic mean relaxation time (corresponding to the mean time of the lognormal function), τ_{CAP}, of the α_c relaxation. Note that these values were fixed to be constant until approximately the times indicated by arrows. Temperatures: 162 K (triangles), 160 K (stars), and 158 K (squares). Vertical lines are meant as guides for the eye only.

over this range. However, at large times, where a_{AP} is already 0, we observe a peak in a_{CAP} followed by slow decay showing that there is a slow evolution where a small fraction of the CAP part is additionally immobilized and possibly a small fraction converted into the crystalline phase. Interestingly, as indicated in Figure 10 by arrows, this occurs in the zone where the τ_{CAP} increases significantly (see Figure 10c). These issues will be discussed more thoroughly in the Discussion section.

3.5. Temperature Modulated Differential Scanning Calorimetry (TMDSC). In order to investigate the crystallization behavior and the accompanying CAP phase in more detail, we also employed temperature modulated differential scanning calorimeter (TMDSC) which provides thermal information under quasi equilibrium conditions.

Figure 11a shows the reversible part of the specific heat capacity C_p^{rev} of two subsequent heating ramps of d-PDMS obtained under a temperature modulation of ±0.5 °C/min superimposed on a 2 K/min heating ramp. The first ramp represents the thermal behavior of the supercooled liquid (glass) demonstrating the typical abrupt glass transition transition followed by a sharp decrease at about 180 K associated with the onset of crystallization. The subsequent heating ramp is then obtained after cooling the sample down to 93 K from 228 K (before the melting transition) and represents the semicrystalline material. As observed, the heat capacity is much lower than that of the supercooled amorphous liquid but still a small broad jump is observed between 145 and 175 K. This is another evidence of the modified amorphous phase (CAP) which is in agreement with the dielectric data showing a slower relaxation and a very broad relaxation spectrum (see Figure 8b).

Furthermore, by applying a sinusoidal modulation of ±0.5 °C/min on a constant temperature, the quasi-isothermal

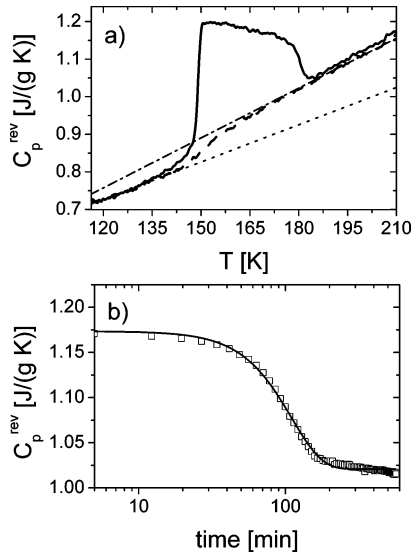

Figure 11. (a) Temperature dependence of the reversible heat capacity C_p^{rev} starting from the glass (solid line) and the semicrystal (broken line) respectively. The data were obtained by cooling (20 K/min) down to 93 K (glassy state) and then heated (2 K/min) up to 230 K allowing crystallization to the final state. The sample was then cooled (20 K/min) down to 93 K and then slowly heated (2 K/min). The dotted and dash-dotted lines display the extrapolated heat capacities from the glass and the high-temperature side of the semicrystalline state respectively. (b) Quasi-isothermal crystallization kinetics of d-PDMS obtained from TM−DSC. Time dependence of the reversible part of the specific heat capacity, C_p^{rev}, obtained under a temperature modulation of ±0.5 °C/min under quasi-isothermal conditions at 162 K. The solid line displays a fit using an Avrami equation (see text for details).

crystallization kinetics can be determined. This is demonstrated in Figure 11b for $T = 162$ K. As before, the data can be analyzed using a Avrami like law: $C_p^{rev}(t) = (C_p^{rev}(0) - C_p^{rev}(\infty))\exp(-(kt)^n) + C_p^{rev}(\infty)$. The results show that this description is working reasonably well yielding a growth exponent, n, resulting in a value of $n \approx 2.1$ which is not far from what has been found before using WANS.

4. Discussion

Crystalline Structure. WANS shows that, on the local scale, the final crystalline structure essentially does not depend on the temperature. In all cases, the crystal reflections remain essentially on the same position and correspond very nicely with the work of Albouy[25] where the structure proposed is a 4-fold helices organized in a tetragonal crystal lattice. The final degree of crystallinity was found to vary very slightly with the crystallization temperature, increasing from approximately 29 to 33% when the temperature is changed from 158.4 to 169.4 K. This could simply be related to very slow secondary crystallization processes which hinder the observation of the maximum degree of crystallinity within the experimental time scale. The small dependence on temperature may also be an indication of an intrinsic crystal thickening process driven by the reduction in the interfacial free energy. Indeed comparing with the data from SANS, we see that the lamellar spacing increases from approximately 50 Å at 162 K to 59 Å at 168 K. This is accompanied by an apparent increase in the lamellar coherence length from about 59 to 67 Å for the same temperatures. This might indicate a slight perfection of the crystal structure. Note that the coherence length is comparable with the lamellar spacing itself which means that only a few lamellar repetitions occurs within each crystal grain domain. It is worth mentioning that this is compatible with recent sugges-

tions of Strobl proposing a general blocky substructure of polymer lamellas.[2]

It is also interesting to address the local structure of the amorphous phase. The dielectric data have shown a dramatic effect of the dynamics of this phase upon crystallization, however no deviation from the conventional amorphous scattering has been seen by WANS. This means that the local differences of CAP and AP are small, and effects such that as small density differences are not detectable within the accuracy of WANS which is sensitive up to about 10−15 Å. It also might mean that the large effects shown in BDS are caused by anchoring of some random chain segments to small crystal nuclei without involving any strong reorganization processes. Such scenario would also exclude a distinct mesomorphic phase acting as a precursor for crystallization. This is different than observed for PE where a distinct intermediate phase have been seen by WAXS.[10] A more detailed discussion of this subject is given later below.

Dynamics and Crystallization. According to the previous discussion, the crystallinity of PDMS obtained in the cold crystallization range amounts to about 30%. This would imply a corresponding reduction of the excess heat capacity when the supercooled liquid is transformed into the semicrystalline material. This can be calculated by the ratio: $(C_p^{rev}(\text{liquid}) - C_p^{rev}(\text{semicrystal}))/(C_p^{rev}(\text{liquid}) - C_p^{rev}(\text{crystal}))$ which, using the data in Figure 11a at 162 K, gives a value of about 0.8 which is much larger than the expected value of approximately 0.33 from WANS. Here we have used the value of C_p^{rev}(crystal) as the extrapolated value of the experimental data from the glassy state (see dotted line in Figure 11a). Even by using the value of C_p^{rev}(semicrystal) determined from the high-temperature behavior (see dotted−dashed line in Figure 11a), we still obtain a value larger than 0.7, which is clearly not the case.

A way to understand this apparent discrepancy is by noting that the amorphous-like regions connected to crystal lamellas are much more constrained than in the amorphous bulk phase (hence the name CAP) and therefore do not equally contribute to C_p. In other words, the heat capacity measurements are not able to separate the reduction of the specific heat capacity due to the formation of a crystal lattice and the reduced mobility of the intermediating amorphous like chains. A crude estimate of this reduced mobility can be done by calculating $(C_p^{rev}(\text{CAP}) - C_p^{rev}(\text{crystal}))/((C_p^{rev}(AP) - C_p^{rev}(\text{crystal}))(1 - X_c)) = 0.35$, i.e., the reduced mobility leads to decrease of ΔC_p^{rev} of about 65% relative to the value of the pure ordinary amorphous phase.

In this connection it is also interesting to compare the properties of the ordinary amorphous phase and the CAP in terms of the fragility, this time in using the thermodynamic fragility defined as follows:[42]

$$m_{TD} = 1 + \frac{\Delta C_p^{rev}(T_g)}{S_{ex}(T_g)} \tag{12}$$

where $\Delta C_p^{rev}(T_g)$ and $S_{ex}(T_g)$ are the excess heat capacity and configurational entropy at the glass transition. Even though these values are not easily deduced for the conventional amorphous phase due to the crystallization, we can use the current data to evaluate the values of the CAP. Using the extrapolated lines from the glass and semicrystal in Figure 11a, we obtain $\Delta C_p^{rev}(T_g) \approx 0.048$ J/gK and $S_{ex}(T_g) \approx 7.07 \times 10^{-3}$ J/gK, which gives $m_{TD}^{CAP} \approx 6.8$. Here we have used $S_{ex}(T_g) \approx \int_{T_K}^{T_g} \Delta C_p \, d(\ln T)$ and then assumed that for simple polymers, such as PDMS, the Vogel temperature (see Table 1) and the Kauzmann, T_K temperature are identical.[42] Using values available from Wunderlich and co-workers in the literature,[37] we obtain $m_{TD}^{AP} \approx 9.3$ for the fully amorphous material. These values can be compared from the values of the dynamics (eq 8 and Table 1) using the relation[42] $m = \log(\tau(T_g)/\tau_0)m_{TD}$ which gives according to the definition $\tau(T_g) \equiv 100$s, $m^{AP} \approx 133$ and $m^{AP} \approx 100$. Considering the values obtained before ($m^{AP} \approx 154$ and $m^{CAP} \approx 95$), we see a rather good agreement demonstrating once again that the CAP has a "stronger" nature than that of the conventional amorphous phase.

More comparison can be made using the dielectric data. Figure 8b has clearly shown that upon crystallization the relaxation features of the conventional amorphous phase disappear and are replaced by a very broad α_c-relaxation process extending over about 7 orders of magnitude in frequency. Considering the dielectric strength values, our results show that, upon crystallization at 158 K, $\Delta\epsilon$ decreases from 0.62 in the fully amorphous phase to about 0.26 in the final semicrystalline state. If the reduction only were due to crystallization, i.e., where segments implemented into the crystal were completely immobilized while the others keep their amorphous mobility, this would suggest a crystallinity of about 60%. Thus, it is evident that the contribution of CAP to the dielectric strength is smaller than that of AP. Because the lack of a good microscopic model for the dielectric relaxation around the glass transition the interpretation of this comparison is not obvious. Nevertheless, one could consider that the observed reduction is directly connected with the reduction of the effective dipole moment reorientation due to the more restricted environment. In this interpretation we can estimate the effective dipole moment reduction according to $\Delta\epsilon \sim \mu^2 N/V$, where N/V is the density of dipoles. Assuming that the density is not changing and using the degree of crystallization from the WANS measurements, we can calculate $\mu_{CAP}/\mu_{AP} \approx \sqrt{\Delta\epsilon_{CAP}/(\Delta\epsilon_{AP}(1-X_c^{WANS}))} \approx 0.8$, i.e., the effective dipole moment reduction in the CAP amounts to about 20%.

The dynamic experiments have shown that the crystallization is accompanied by a disappearance of the conventional amorphous phase and simultaneously emergence of a different more restricted amorphous phase. This is manifested in much slower molecular motions and a very heterogeneous character. It is reasonable to consider two main potential effects responsible for this behavior: (i) geometric confinement and (ii) grafting/cross-linking of amorphous chain segments on the crystal interfaces.

Considering the first effect, SANS measurements have indicated that the confining region, i.e., the inter lamellar thickness l, would be of the order of about 35−41 Å ($l \approx (1 - X_c)d_{lam}$). Recent studies have shown that the effects of confinement are not expected to be observed before approaching a characteristic length scale of cooperativity which for typical flexible polymers takes a value much smaller of about 10−15 Å in the region around the glass transition, $T = T_g - 1.25T_g$.[39] Additionally, in this framework, the dynamics would be faster if the cooperativity length is approached—in this case rather the contrary is observed.

This leads us to the second point concerning chain pinning/grafting of chains and even cross-linking between small crystalline nuclei/ crystalline structures. This naturally leads to much slower dynamics as the fluctuations of the chains is severely damped, and for chains fixed in more than one point, the chain is effectively forced to fluctuate only between two linkage points and therefore much more constrained. As PDMS is very flexible, the frequency of folding is large which is likely

to lead to effective short strands between the anchoring points without necessarily forming ties between adjacent crystal lamellas. In addition since the dynamics is very fast, any obstruction point would drastically affect the effective time scales. This is likely to be the reason for the large decoupling, i.e., separation in the time scale between the AP and CAP. Similar features have been seen for other flexible polymers such as poly(L-lactic acid) (PLLA)[19,22] and poly(3-hydroxybutyrate)-(PHB),[20,21] but in the case of more rigid polymers like poly-(ethylene terephthalate)(PET)[17,18] and poly(propylene succinate),[15] a more gradual change in the characteristic relaxation time and broadening is observed. It is interesting to compare this behavior with the reduction in the effective dipole moment deduced from BDS. Using our results we have obtained an effective dipole reduction of $\Delta\mu/\mu \approx 20\%$ which can be compared using the results of PET from Alvarez et al.,[18] essentially the same $\Delta\mu/\mu \approx 20\%$ is observed. In this connection, we note that in terms of the fragility index, it is generally observed that for more stiff polymers, the amorphous phase undergoes a significant "fragile−strong" transition whereas for flexible polymers the reduction is much smaller.[41] However as the discussion above shows, this cannot simply be related to the change in the dipole moment $\Delta\mu$ alone but likely is related also to the statistics of the polymer.

It also worth mentioning that the appearance of a distinct slower amorphous dynamics may also be induced by a sort of precrystalline order or mesomorphic phase which acts as a precursor to crystallization. Such ideas have indeed been proposed although along different lines, proposing bundle-like structures,[3] and a spinodal liquid−liquid transition (isotropic−nematic) preluding the formation of real crystals. Although such scenarios cannot be excluded from the BDS alone, the WANS structural results show no indication of such entities where the scattering at all times can be described by a sum of a (fixed) amorphous and crystalline contribution. However as such structures should be more apparent from a combination of kinetic data, we postpone the discussion of this to the next section.

Crystallization Kinetics. In the analysis above using eq 9, the dielectric response was shown to be described well with a linear superposition of two relaxation contributions, we therefore might expect that the loss of the amorphous part is directly related to the crystalline fraction given by WANS. In Figure 12, the relative crystallinity, deduced directly from the WANS experiments and indirectly from the loss of the conventional amorphous phase from BDS is compared.

Even though the data displayed are not obtained under precisely the same conditions and the temperature is not exactly the same, the curves displayed in Figure 12a coincide rather well, especially at lower temperatures and longer times. The evident time shift observable for the highest temperature investigated, can be attributed to the difficulties in defining the initial time when the crystallization occurs somehow on a time scale comparable to the time needed to record a single curve. When plotting the same data on an Avrami representation (Figure 12b), i.e. when $\ln(-\ln(1 - X_c(t)/X_c(\infty))$ is plotted vs logarithmic time axis, a systematic difference is observed. First of all, the data from WANS display a clear linear behavior in the primary crystallization regime, while the BDS data show a distinct curvature. In order to rationalize the differences, one has to take into account that whereas the WANS data directly give the amount of crystals and are therefore initially described by an Avrami-like nucleation and growth mechanism, the BDS results display a progressive disappearance of the conventional

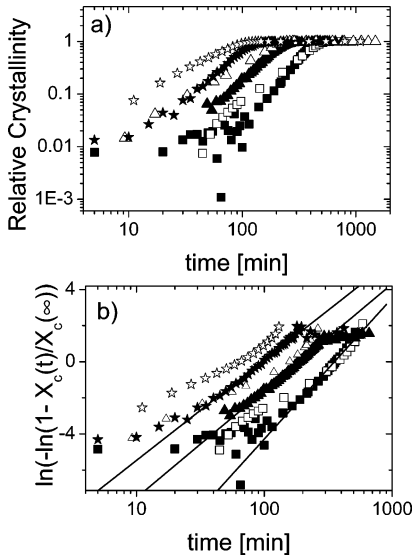

Figure 12. Crystallization kinetics deduced from structural measurements (WANS, filled symbols) and local mobility measurements (BDS, open symbols). (a) Log−log plot of the relative crystallinity deduced from the loss of the conventional amorphous phase ($X_c(t)/X_c(\infty) \sim 1 - a_{AP}(t)/a_{AP}(t = 0)$) and WANS measurements. Temperatures are 158 K (squares), 160 K (triangles) and 162 K (circles). The temperatures of WANS are systematically about 0.4 K above those of the WANS. (b) same data as in part a but in the so-called Avrami representation, i.e., where $\ln(-\ln(1 - X_c(t)/X_c(\infty))$ is plotted on a log t time scale. Note that even though data is obtained after approximately the same thermal history was applied, the measurements were not performed simultaneously.

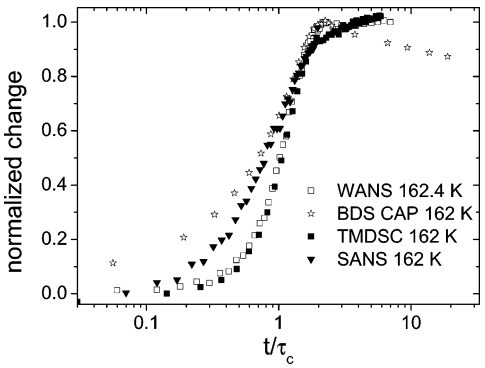

Figure 13. Comparison of the apparent crystallization kinetics as deduced from SANS, WANS, BDS, and TMDSC on a linear-logarithmic presentation. Please note that in order to facilitate the comparison, the horizontal time axis has been rescaled using the characteristic crystallization time, τ_c determined from the inflection point of the kinetic curves. This is convenient because although the samples share approximately the same thermal history, the data have not been obtained under identical conditions and therefore most notably the temperature may be subject to systematic variations.

amorphous phase which undergoes a more complicated transformation. Additionally, in the simple analysis of the dielectric data $\Delta\epsilon$ of each process was taken as constant which is true if the phases are uncoupled and the jump in the dielectric strength is discrete. Furthermore, as already commented above, the disappearance of the conventional amorphous phase is coupled with the emergence of the CAP signal as well as the crystalline phase.

These features are compared in more detail in Figure 13, where the time evolution of the properties associated with the crystalline formation is displayed for all three techniques: normalized fraction of CAP seen by BDS, the relative crystallinity measured by WANS, the normalized change in the invariant from SANS (eq 6) and the normalized heat capacity

change deduced from TMDSC. For direct comparison the data have been plotted on a time scale normalized to the characteristic crystallization time, τ_c, which has been deduced from the inflection points of the kinetic curves (maximum of the first derivative).

As seen the DSC and the WANS curves seem to evolve in parallel following the same behavior except at long times. However, when comparing with BDS, it seems that at the very early stages the increase in the BDS signal is substantial before any significant increase in the crystalline phase is observed by WANS. Such effect could not simply come from the differences in conditions (temperature), as this is effectively normalized out via τ_c, but must be an intrinsic behavior. Essentially the same picture has been seen on another polymer system by Wurm et al.,[16] where this behavior was taken as a signature of some preordering of the amorphous phase. Another possible picture to account for such behavior is to consider that at the early stages of crystallization only small crystalline-like nodules/aggregates (also termed "baby-nuclei"[12,13]) appear. Although these nodules would correspond to a very small amount of crystalline material, they would act as anchoring points of the PDMS chains and therefore affect significantly the mobility of the surrounding segments. These anchorage-affected segments would not longer contribute to the dielectric signal as in the conventional AP but to that identified as originated in the CAP. The further growing of these nodules to form the lamella-like crystals detectable by WANS will increase the amount of the CAP phase and made the conventional AP to finally disappear at long enough times. In this view, the effect of the chain anchorage would extend over a relative large number of interconnected chain segments.

At this point, it is interesting to compare these results of a lamellar diblock polymer PDMS−PS where the anchorage effects indeed were found to be noticeable up to about 2 nm from the lamellar wall.[23] Using this value, we can estimate an upper limit of the signal that would be detectable by BDS but not by WANS. Assuming that the crystal growth occurs from point like randomly distributed centers (i.e., essentially zero crystallinity) with a mean distance which is identical with the periodicity of the later developed crystal lamellas. Using $d_{lam} \approx 5$ nm from SANS at 162 K, we obtain a fraction of about $\approx 2^3/5^3$ which gives a value of approximately 6% of CAP which comparing with the final ≈70% of CAP implies of about 10% of the dielectric signal of the CAP in the initial stage of the crystallization. Now considering the comparison already displayed in Figure 12, we see that this value corresponds rather closely with the observed differences in the kinetics of crystallization by BDS. It is tempting to conclude that this is also seen by SANS where the signal shows a tendency to appear before the WANS perhaps suggesting that the CAP formation gives a sufficient contrast at large scales in terms of density fluctuations already at these short times. However, as the data at short times as well as the data normalization at short times in SANS is difficult, a final conclusion cannot be reached at this point. In any case, it should be pointed out that the SANS curves during the kinetic experiments (see Figure 7a) show an increase of the intensity without any displacement of the correlation peak, which seems to indicate that the crystals grow from fixed nuclei and no significant nucleation occurs during crystallization. Such a scenario would be compatible with athermal nucleation and growth mechanism which would predict a Avrami growth law with exponent $n = 3$ which indeed is very close to what has been found from the fitting of the WANS results seen in Figure 5b, where values between 2.7 and 3.2 were found.

Following up the discussions in the sections above, it is also tempting to consider inherent effects as precursors such a slight pre-ordering effect acting as a sort of precursor for the nucleation. Although the crystalline nodules discussed above can be regarded as a precursor state in relation to the fully developed crystal, one could also imagine more distinct mesomorphic structures/states suggested earlier.[3,7,9,16] Precursors have been reported to be seen directly during crystallization by dielectric spectroscopy in another system where the CAP and AP are not as strongly decoupled[15] and also indirectly by measuring the crystallization kinetics of initial fully amorphous PET samples having different thermal histories.[40] However, in the latter study, an Avrami exponent of about 3 was found, which is close to what has been found in this work, which can be viewed as traditional nucleation and growth favoring that the precursors are essentially small prevailing crystalline nuclei entities that cannot be resolved within the detection limit of wide angle scattering techniques. Similar ideas have been made by Wang et al. where in a simultaneous study of WAXS/SAXS the appearance of a correlation peak in the SAXS data before appearance of WAXS signal was attributed to a lower sensitivity of the latter technique. It is also evident from the current data in Figure 13 that the SANS signal appears to be closer to the BDS data than the WANS showing that nuclei for the crystallization seriously affecting the BDS data also is observed by SANS before WANS.

Now, focusing on the long time behavior of the crystallization process, we observe a significant drop in the fraction of CAP which is to a certain degree accompanied by a very slight increase of the crystalline fraction as observed by WANS. This occurs in the secondary crystallization regime, where most of the crystallization have occurred and most of the conventional amorphous phase is consumed. Recalling Figure 10, we see that this is accompanied by an increase in the characteristic relaxation time of the α_c-process. This may be interpreted as follows—as the lamellas start to overlap in the secondary crystallization regime—the dynamics is so restricted that further growth can only come from some loose chains located at the crystal fronts. These chains may attach and form cross-link to the next evolving crystal, leading to a slightly larger crystallinity but mostly a even slower overall mobility and consequently lower $\Delta\epsilon$. This is predominantly most likely to happen to chains that are loose and hence fastest, which would explain the slight shift in the α_c-process observed in Figure 9b and the consequent increase of τ^* (Figure 10c). However comparing the increase in the X_c with the decrease of the CAP fraction, it is likely that most of the CAP does not incorporate into the crystal but become further restricted and slower such that $\Delta\epsilon$ is reduced. Similar results have been found for PET in a simultaneous X-ray and dielectric spectroscopy study.[17] This phenomenon can be further investigated using the TMDSC data displayed in Figure 13. At long times, an extremely slow evolution of C_p^{rev} is observed which is qualitatively similar to the behavior observed for the CAP response by BDS. Hence it is likely that the slow decay in C_p^{rev} at long times also reflects modifications in the CAP which due to its slow dynamics experiences an increasingly difficulty to move between lamellar fronts. It is noteworthy that the TMSDC curve does not show significant differences respect to the WANS data at fast times, contrary to the CAP behavior. This finding is likely originated by the fact that the TMDSC data normalization were performed using as initial C_p^{rev} value that obtained from the Avrami fitting, due to the experimental difficulties in determining it directly. Therefore, the small but systematic deviations of the initial part of the dielectric kinetic data from

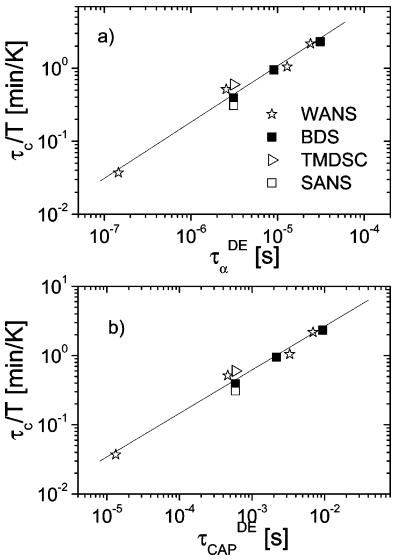

Figure 14. Correlation between the characteristic normalized crystallization time, τ_c/T, and (a) the typical time scale of the α-relaxation of the conventional AP, τ_α^{DE} and (b) the relaxation associated with the CAP, α_c-relaxation, τ_{CAP}^{DE}. Note that the data are presented on a log−log scale. The straight lines displayed represent a power law with exponent, $y = 0.77$ and 0.62 in (a) (AP) and (b) (CAP), respectively.

the Avrami equation could not be detectable in the TMDSC data.

Correlation between Crystallization Kinetics and Segmental Dynamics. The WANS data show that PDMS starts to cold crystallize on practical time scales in a region of about 10 K above T_g. The characteristic crystallization time is found to be drastically dependent on the temperature and change by nearly 1 order of magnitude by changing the temperature some few degrees. This suggests a strong correlation between the crystallization time, τ_c, and the typical time scale of the α-relaxation, τ_α^* being the main dynamic process around T_g. Indeed it has been claimed that the kinetic part of crystallization rate scales with the self-diffusion of the molecules.[43] It is therefore interesting to check the validity of the Stokes−Einstein equation which in this case would imply an inverse linear relationship between the crystallization time, τ_c and the friction coefficient, *f*. However, as the crystal ordering do not necessarily involve large scale organizational processes, it is reasonable to assume that *f* can be more accurately estimated by the segmental diffusion characterized by the alpha relaxation, i.e., $f \approx 1/\tau_\alpha^*$. On the other hand, it is known that, close to the glass transition, this relationship generally fails,[44] and the equation needs to be modified to yield a more general fractional law, which in this case we may write as follows: $\tau_c \sim T(\tau_\alpha^*)^y$, where *y* is constant and $y \leq 1$. However, here it should be pointed out that the cold crystallization is a driven diffusion process subject to a thermodynamic gradient in terms of the degree of supercooling relative to the crystallization temperature.

In any case the correlation between the typical reduced crystallization time, τ_c/T, and the characteristic relaxation time of the AP, τ_α^{DE}, and the CAP, τ_{CAP}^{DE} is given for temperatures, $T < 1.15T_g$, in Figure 14. The former, τ_c, can be deduced from the first derivative of the kinetic curves. Extracting the correlation exponent, a value of about $y = 0.77 \pm 0.07$ is obtained for the conventional amorphous phase which indeed suggest a decoupling of the local friction and the segmental diffusion and thus a breakdown of the Stokes−Einstein law.

Alternatively, according with the previous discussion, one could consider that the CAP dynamics that controls the crystallization. In this way we obtain a similar power law exponent: $y = 0.62 \pm 0.05$. Similar values have earlier been obtained in both polymeric and low molecular weight materials deduced from the scaling between the self-diffusion and the viscosity coefficients,[43] between the kinetic part of crystallization rate and viscosity,[44] and also between the crystallization rate and the characteristic time of the α-relaxation.[21] However, in order to conclude more on this matter in a consistent quantitative way, the thermodynamic driving force needed to be determined and decoupled from the kinetic part of the crystallization rate as has been done in ref 44 for low molecular weight compounds.

5. Conclusion

In this paper an extensive study of the crystallization behavior of an archetypical flexible model polymer has been presented. A special emphasis has been made to understand the relationship between dynamics and structure evolution. This has been done using a range of techniques, WANS and SANS to study the local and mesoscopic structure before, under and after crystallization. This is compared with the local dynamical mobility using broadband dielectric spectroscopy and temperature modulated differential scanning calorimetry.

The data seem to support the usual nucleation and growth mechanism showing a typical Avrami like growth curves displaying a exponent $n \approx 3$ which is compatible with an athermal nucleation and three-dimensional growth mechanism. This is also compatible with the SANS data where the correlation peak seem to be growing homogeneously in time without any shift in the position of the maxima.

Combining results from BDS and WANS we see that the amorphous phase decays in parallel with the appearance of a well-defined crystalline phase. However, at short times, we observe a slight indication that the amorphous phase, seen by BDS, is altered before any significant crystallinity is detected by WANS. This can be attributed to the presence of a small fraction of crystalline point-like centers/nuclei that predominantly act as attachment point of chain segments. Such restrictions would clearly affect the dynamics without any strong associated change in crystallinity which explains the stronger dependence of the dielectric constants as a function of time. It could also mean a signature of a slight pre-ordering process or mesomorphic phase preluding the final crystalline phase; however, no such phenomena seem to be absolutely necessary to explain the current data. At longer crystallization times, these restrictions imposed on the remaining mobile amorphous become more and more evident with an increasing amount of a modified "constrained amorphous phase" (CAP) which finally, at the end of the crystallization process, contains all of the uncrystallized chains. The resulting dynamics of CAP is about 3 orders of magnitude slower than the ordinary α-relaxation. This slow and heterogeneous dynamics cannot be attributed to confinement effects as the confining lamellar thickness length is relatively large (about 35−41 Å) and such effects would be expected to enhance the relaxation times. Instead it can be associated with the amorphous chains grafted to the emerging crystalline parts. A characteristic behavior of the current system, which is shared with other flexible polymers,[20] is the apparent decoupling of the ordinary amorphous phase and the CAP. This is reflected in a well-separated constant characteristic time of the two processes during the primary crystallization regime. We attribute this behavior to the high flexibility of the PDMS backbone, giving rise to large probability to form loops which will have different well-separated dynamics induced by the junctions points in comparison with the more free chains

displaying bulk behavior. It is also interesting to note that after most of the crystallization has occurred, in the secondary crystallization regime, a fraction of the dielectric CAP signal very slowly decays and the most probable relaxation time shifts toward longer times. The change of the dynamics can be attributed to a very slow conversion of the faster (free ends) fraction of CAP attaching to other emerging crystal and consequently may form trans-lamellar cross-links.

In summary, the results point toward the following picture. At very early times, crystalline ("baby-like") nuclei are homogeneously formed in the system. This causes a constraint on the surrounding chains connected to these crystalline nuclei. This is manifested as a distinct relaxation contribution that is drastically slower and heterogeneous than the ordinary amorphous α-relaxation of the melt. This would also explain a signal in SANS before any accompanying crystallization signal in WANS. Once the crystal starts developing, the CAP fraction grows and the ordinary amorphous phase gradually disappears. At the very end, the growing crystalline fronts start to overlap and some of the remaining CAP becomes even more constrained due to cross-link strongly manifested in the dielectric response and the heat capacity.

Acknowledgment. The authors acknowledge the University of the Basque Country, the Basque Country Government (A9/UPV 00206.215-13568/2001), and the Spanish Ministery of Education (MAT 2004-01617) for support. The support of the European Community within the SoftComp Network of Excellence (NoE) program (Project No. NMP3-CT-2004-502235) is also acknowledged. Allocation of beamtime and support for the measurements carried out at the D11 and D1B instruments by ILL/NMI3 and the Spanish Initiative for Neutron Scattering (SpINS) respectively are greatly appreciated. The authors are also indebted to Dr. Lutz Willner for performing the GPC measurements of the polymer sample.

References and Notes

(1) Sommer, J. U. S., Reiter, G., Eds. *Polymer Crystallization: Observations Concepts and Interpretations*; Springer-Verlag: Berlin, 2003.
(2) Strobl, G. *Prog. Polym. Sci.* **2006**, *31*, 398.
(3) Allegra, G.; Valdo Meille, S. *Adv. Polym. Sci.* **2005**, *191*, 87.
(4) Gedde, U. W. *Polymer Physics*; Kluwer: Dordrecht, The Netherlands, 1999.
(5) Hippler, T.; Jiang, S.; Strobl, G. *Macromolecules* **2005**, *38*, 9396.
(6) Sirota, E. B. *Macromolecules* **2007**, *40*, 1043.
(7) Imai, M.; Kaji, K.; Kanaya, T. *Phys. Rev. Lett.* **1993**, *71*, 4162.
(8) Terrill, N. J.; Fairclough, P. A.; Towns-Andrews, E.; Komanschek, B. U.; Young, R. J.; Ryan, A. J. *Polymer* **1998**, *39*, 2381.
(9) Olmsted, P. D.; Poon, W. C. K.; McLeish, T. C. B.; Terril, N. J.; Ryan, A. J. *Phys. Rev. Lett.* **1998**, *81*, 373.
(10) Sajkiewicz, P.; Hashimoto, T.; Saijo, K.; Gradys, A. *Polymer* **2005**, *46*, 513.
(11) Wang, Z.-G.; Hsiao, S. B.; Sirota, E. B.; Agarwal, P.; Srinivas, S. *Macromolecules* **2000**, *33*, 978.
(12) Muthukumar, M.; Welch, P. *Polymer* **2000**, *41*, 8833.
(13) Welch, P.; Muthukumar, M. *Phys. Rev. Lett.* **2001**, *87*, Art.No. 218302.
(14) Ezquerra, T. A.; Majszczyk, J.; Baltá-Calleja, F. J.; López-Cabarcos, E.; Gardner, K. H.; Hsiao, B. S. *Phys. Scr.* **1994**, *T55*, 212.
(15) Soccio, M.; Nogales, A.; Lotti, N.; Munari, A.; Ezquerra, T. A. *Phys. Rev. Lett.* **2007**, *98*, 037801.
(16) Wurm, A.; Soliman, R.; Goossens, J. G. P.; Bras, W.; Schick, C. J. *Non-Cryst. Solids* **2005**, *351*, 2773.
(17) Ezquerra, T. A.; Sics, I.; Nogales, A.; Denchev, Z.; Baltá-Calleja, F. J. *Polymer* **2004**, *45*, 3953.
(18) Alvarez, C.; Sics, I.; Nogales, A.; Denchev, Z.; Funari, S. S.; Ezquerra, T. A. *Polymer* **2004**, *45*, 3953.
(19) Mijović, J.; Sy, J.-W. *Macromolecules* **2002**, *35*, 6370.
(20) Napolitano, S.; Wübbenhorst, M. *Macromolecules* **2006**, *39*, 5967.
(21) Napolitano, S.; Wübbenhorst, M. *J. Phys. Chem. B* **2007**, *111*, 5775.
(22) Brás, A. R.; Viciosa, M. T.; Wang, Y.; Dionśio, M.; Mano, J. F. *Macromolecules* **2006**, *39*, 6513.
(23) Lorthioir, C.; Alegría, A.; Colmenero, J.; Deloche, B. *Macromolecules* **2004**, *37*, 7808.
(24) Damaschun, G. *Kolloid-Z* **1962**, *180*, 65.
(25) Albouy, P.-A. *Polymer* **2000**, *33*, 3083.
(26) Sundararajan, P. R. *Polymer* **2002**, *43*, 1691.
(27) Feio, G.; Cohen-Addad, J. P.; Buntinx, G. *J. Polym. Sci., B: Polym. Phys.* **1989**, *27*, 1.
(28) Maus, A. Ph.D. Thesis, University of Freiburg; 2005; p 65.
(29) Dollase, T.; Spiess, H. W.; Gottlieb, M.; Yerushalmi-Rozen, R. *Euro. Phys. Lett.* **2002**, *60*, 390.
(30) Adachi, H.; Adachi, K.; Ishida, Y.; Kotaka *J. Polym. Sci. B: Polym. Phys.* **1979**, *17*, 851.
(31) Kirst, K. U.; Kremer, F.; Litvinov, V. M. *Macromolecules* **1993**, *26*, 975.
(32) Kirst, K. U.; Kremer, F.; Pakula, T.; Hollingshurst, J. *J. Colloid Polym. Sci.* **1994**, *272*, 1420.
(33) Brandrup, J., Immergut, E. H., Eds. *Polymer Handbook*; John Wiley and Sons: London, 1975.
(34) Lindner, P., Zemb, T., Eds. *Neutrons, X-Ray and Light. Scattering Methods Applied to Soft Condensed Matter*; Elsevier: Amsterdam, 2002.
(35) Pedersen, J. S.; Posselt, D.; Mortensen, K. *J. Appl. Crystallogr.* **1990**, *23*, 321.
(36) The experimental resolution was calculated using the approach given by Pedersen et al.,[35] where the corresponding function is shown to be essentially as a Gaussian function. The width is given by the sum of the individual contributions from the wavelength spread and the smearing in the scattering angle given by the finite beam divergence and detector pixel size. Inserting the instrumental parameters corresponding to the 2.5 collimation-to-sample and 2.5 m sample-to-detector distances (region of which the peak appears), we obtain $\sigma_Q \approx 6 \times 10^{-3}$ Å^{-1} at $Q = 0.1$ Å^{-1}.
(37) Varma-Nair, M.; Wesson, J. P.; Wunderlich, B. *J. Therm. Calor. Anal.* **1989**, *35*, 1913.
(38) Angell, C. A. *J. Non-Cryst. Solids* **1991**, *13*, 131.
(39) Cangialosi, D.; Alegria, A. Colmenero, J. *Phys. Rev. E* **2007**, *74*, 011514.
(40) Kiflie, Z.; Piccarolo, S.; Brucato, V.; Baltá - Calleja, F. J. *Polymer* **2002**, *43*, 4487.
(41) Arnoult, M.; Dargent, E.; Mano, J. F. *Polymer* **2007**, *48*, 1012.
(42) Cangialosi, D.; Alegria, A.; Colmenero, J. *J. Chem. Phys.* **2006**, *124*, 024906.
(43) Mapes, M. K.; Swallen, S. F.; Ediger, M. D. *J. Phys. Chem. B* **2006**, *110*, 507.
(44) Ngai, K. L.; Magill, J. H.; Plazek, D. J. *J. Chem. Phys.* **2000**, *112*, 1887.

MA702055B